XPS investigation of MnO_2 deposits functionalized with graphitic carbon nitride

Mattia Benedet,[1] Alberto Gasparotto,[1,2,a)] Gian Andrea Rizzi,[1,2] Chiara Maccato,[1,2] Davide Mariotti,[3] Ruairi M^{c}Glynn,[3] and Davide Barreca[2]

[1] *Department of Chemical Sciences, Padova University and INSTM, 35131 Padova, Italy*

[2] *CNR-ICMATE and INSTM, Department of Chemical Sciences, Padova University, 35131 Padova, Italy*

[3] *School of Engineering, Ulster University, 2-24 York Street, Belfast, BT15 1AP, UK*

(Received day Month year; accepted day Month year; published day Month year)

Composite materials based on MnO_2 deposits functionalized with graphitic carbon nitride (gCN) nanostructures are promising (photo)electrocatalysts for the oxygen evolution reaction (OER). Besides the individual properties of the two electrode components, mutual interactions at their interface can also exert a significant influence on functional performances. In this work, MnO_2 deposits are synthesized by plasma enhanced-chemical vapor deposition (PE-CVD) on Ni foam supports and subsequently decorated with two different forms of carbon nitride via electrophoretic deposition (EPD). Structural and morphological analyses revealed the formation of β-MnO_2 2D structures hierarchically assembled into flower-like architectures, whose surface appeared decorated by 3D particles built up from gCN nanoflakes. Based on the intimate contact between the two semiconductors, an effective electronic and chemical coupling was established at their interface. In the following, we report on a comparative X-ray photoelectron spectroscopy (XPS) characterization of a bare MnO_2 electrode material and of two MnO_2-gCN composite systems prepared from different carbon nitride powders. Survey spectra, as well as detailed scans for the C 1s, N 1s, O 1s, and Mn 2p regions are presented and critically discussed.

Keywords: MnO_2; gCN; PE-CVD; electrophoretic deposition; X-ray photoelectron spectroscopy

Acccession#: Enter Accession Number.

Technique: XPS

Host Material: MnO_2; MnO_2-gCN(M); MnO_2; MnO_2-gCN(CM)

Instrument: ThermoFisher Scientific Escalab Xi+

Major Elements in Spectra: C, N, O, Mn

Minor Elements in Spectra: none

Published Spectra: 14

Spectra in Electronic Record: 14

Spectral Category: comparison

INTRODUCTION

The increasing use of fossil fuels on a global scale is raising serious concerns not only for the progressive depletion of these non-renewable resources, but also for their manifold detrimental effects on natural ecosystems and human health (Refs. 1-4). In this regard, the development of green catalyst materials, made of abundant elements and capable of efficiently triggering the generation of sustainable energy vectors represents an important global challenge for its techno-scientific, economic and global-health implications (Refs. 1, 2, 5). More specifically, the catalyst-assisted generation of hydrogen from water, possibly activated by sunlight, might revolutionize the current energy infrastructure in a much greener perspective (Refs. 6-10). However, in spite of its huge applicative potential, the efficient H_2O-to-H_2 conversion is still largely dependent on the development of advanced catalytic platforms capable of activating the oxygen evolution reaction (OER), the bottleneck of the overall water splitting process (Refs. 1, 5, 6, 11).

Over the last decade, graphitic carbon nitride (hereafter abbreviated as gCN) has emerged as a promising OER (photo)electrocatalyst, featuring remarkable activity, good chemical and thermal stability, low cost and non-toxicity (Refs. 4, 6, 12, 13). Nevertheless, in spite of its recognized advantages, this material is affected by some drawbacks limiting its functional performances, among which its low surface area, modest electrical conductivity, and rapid recombination of photogenerated charge carriers (Refs. 1, 4, 9, 13, 14). Among the approaches proposed to circumvent such disadvantages, the development of composite systems in which gCN is combined with other semiconductors, controlling the assembly process at the nanoscale, and the immobilization of such systems on porous, highly conductive supports, are considered particularly appealing (Refs. 1, 7, 9, 11, 13, 15, 16).

Within this scenario, in the present contribution we report on the tailored growth of MnO_2-gCN composite systems on Ni foam substrates by a hybrid PE-CVD/EPD synthetic approach. The choice for MnO_2, a low cost and environmental friendly material, is motivated by its narrower band gap with respect to gCN ($E_G \approx$ 2.0 *vs*. 2.7 eV), allowing an extended Vis light absorption, as well as by its band structure that, upon coupling with gCN, might yield the formation of a *Z*-scheme heterojunction, favoring electron/hole separation (Refs. 1, 5, 15, 17, 18). The direct growth of MnO_2-gCN nanostructures on Ni foams favorably impact on the system surface area and amount of active sites, increasing the interfacial contact between the electrode material and the reaction medium (Refs. 5, 9, 11, 17).

More specifically, basing on previously optimized conditions (Ref. 17), MnO_2 was grown on metallic Ni foams by PE-CVD using the precursor $Mn(hfa)_2$TMEDA (hfa = 1,1,1,5,5,5-hexafluoro-2,4-pentanedionate; TMEDA = *N*,*N*,*N'*,*N'*-tetramethylethylenediamine) in Ar/O_2 plasmas. Subsequently, gCN powders, synthesized by thermal condensation of melamine or from the melamine-cyanuric acid adduct (Refs. 6, 19), were deposited on MnO_2 by EPD (Ref. 20) obtaining, in both cases, the decoration of the metal oxide surface by gCN aggregates.

A detailed XPS investigation, complemented by other characterization techniques, revealed that the two gCN forms were highly defective and characterized, in particular, by a

a) Author to whom correspondence should be addressed. e-mail: alberto.gasparotto@unipd.it (A.G.).

considerable amount of uncondensed -NH_x (x = 1,2) groups on the edges of heptazinic rings, whose presence might beneficially affect the system catalytic activity (Refs. 6, 21, 22). Nonetheless, the comparative analysis of XPS results pertaining to bare MnO_2 and the two MnO_2-gCN composites revealed that, for the latter systems, an effective interplay was established at the interface among the two semiconductors, an effect mainly explained basing on the formation of a *Z*-scheme heterojunction, with an electron flow from gCN to MnO_2 (Ref. 15).

SPECIMEN DESCRIPTION (ACCESSION # MnO_2)

Host Material: MnO_2

CAS Registry #: unknown

Host Material Characteristics: homogeneous; solid; polycrystalline; semiconductor; inorganic compound; Thin Film

Chemical Name: Manganese (IV) oxide

Source: sample prepared by PE-CVD of MnO_2 on a Ni foam substrate, followed by air annealing at 400°C for 1 h.

Host Composition: C, O, Mn

Form: Supported thin film

Structure: X-ray diffraction (XRD) analysis evidenced two relatively broad reflections at 2θ ≈28.5° and 37.2°, ascribed to the (110) and (101) crystallographic planes of β-MnO_2 (Refs. 2, 23, 24). The presence of this polymorph was also confirmed by Raman spectroscopy measurements, evidencing signals at ≈570 cm^{-1} and 630 cm^{-1} attributable to the Mn-O stretching vibrations of manganese dioxide (Refs. 3, 5, 18, 25). Scanning electron microscopy (SEM) analyses revealed that the deposit consisted of interconnected β-MnO_2 lamellar structures assembled into 3D flower-like architectures characterized by a high surface area (see the inset in figure Accession # NFigA01).

History & Significance: The MnO_2 deposit was grown on a pre-cleaned Ni foam substrate in a custom-built PE-CVD apparatus equipped with a 13.56 MHz radio frequency (RF) generator (Ref. 17). The compound $Mn(hfa)_2TMEDA$ (hfa = 1,1,1,5,5,5-hexafluoro-2,4-pentanedionate; TMEDA = *N*,*N*,*N'*,*N'*-tetramethylethylenediamine) (Ref. 26) was used as precursor in Ar/O_2 plasmas. Basing on previous results (Ref. 17), the following optimized conditions were adopted: growth temperature = 300 °C; RF-power = 20 W; total Ar flow rate = 65 standard cubic centimeters per minute (sccm); total O_2 flow rate = 5 sccm; total pressure = 1.0 mbar; duration = 3 h. The obtained sample was finally annealed in air at 400°C for 1 h.

As Received Condition: as grown

Analyzed Region: same as host material

Ex Situ Preparation/Mounting: Sample was fixed by a conductive copper tape and a metallic clip on a grounded sample holder, and introduced into the analysis chamber through a fast entry lock system.

In Situ Preparation: none

Charge Control: No flood gun was used during analysis.

Temp. During Analysis: 298 K

Pressure During Analysis: $<10^{-8}$ Pa

Pre-analysis Beam Exposure: 120 s.

SPECIMEN DESCRIPTION (ACCESSION # MnO_2-gCN(M))

Host Material: MnO_2-gCN(M)

CAS Registry #: unknown

Host Material Characteristics: homogeneous; solid; polycrystalline; semiconductor; composite; Thin Film

Chemical Name: Manganese (IV) oxide-graphitic carbon nitride

Source: sample prepared by PE-CVD of MnO_2 on a Ni foam substrate, followed by functionalization with gCN via EPD and final air annealing at 400 °C for 1 h.

Host Composition: C, N, O, Mn

Form: Supported nanocomposite thin film

Structure: XRD measurements on the MnO_2-gCN(M) composite sample yielded a diffraction pattern very similar to the one of bare MnO_2 (see sample accession #MnO_2), indicating thus that gCN deposition did not appreciably affect the structural features of the underlying metal oxide. Nonetheless, the peak at ≈28.5° appeared further broadened towards lower 2θ values, an effect attributable to the partial overlap with the (002) gCN reflection (Refs. 1, 6). SEM analyses (see the inset in figure Accession # NFigB01) evidenced the presence of irregularly shaped carbon nitride aggregates (dimensions = 1-10 μm) partially covering the above described MnO_2 structures.

History & Significance: Deposition conditions for MnO_2 were the same adopted for the previous accession. Subsequently, gCN(M) powders were synthesized by thermal condensation of melamine following a previously reported procedure (Ref. 6), and hence deposited onto MnO_2 by EPD (Ref. 20) adopting an applied potential of 5 V and a deposition time of 180 s. The obtained sample was finally annealed in air at 400 °C for 1 h.

As Received Condition: as grown

Analyzed Region: same as host material

Ex Situ Preparation/Mounting: Sample was fixed by a conductive copper tape and a metallic clip on a grounded sample holder, and introduced into the analysis chamber through a fast entry lock system.

In Situ Preparation: none

Charge Control: No flood gun was used during analysis.

Temp. During Analysis: 298 K

Pressure During Analysis: $<10^{-8}$ Pa

Pre-analysis Beam Exposure: 120 s.

SPECIMEN DESCRIPTION (ACCESSION # MnO_2-gCN(CM))

Host Material: MnO_2-gCN(CM)

CAS Registry #: unknown

Host Material Characteristics: homogeneous; solid; polycrystalline; semiconductor; composite; Thin Film

Chemical Name: Manganese (IV) oxide-graphitic carbon nitride

Source: sample prepared by PE-CVD of MnO_2 on a Ni foam substrate, followed by functionalization with gCN via EPD and final air annealing at 400 °C for 1 h.

Host Composition: C, N, O, Mn

Form: Supported nanocomposite thin film

Structure: Sample characterization by XRD yielded results very similar to the previously described composite (see sample accession #MnO_2-gCN(M)). Nevertheless, SEM measurement revealed that gCN formed well-defined spherical aggregates with a narrower size distribution (1-3 μm) and a more homogeneous dispersion over MnO_2 surface (see the inset in figure Accession # NFigC01).

History & Significance: Deposition conditions for MnO_2 were the same adopted for the previous two specimens. Subsequently, at variance from sample accession #MnO_2-gCN(M), gCN(CM) powders were synthesized by thermal condensation of a melamine-cyanuric acid adduct following a previously reported procedure (Ref. 19), and then deposited onto MnO_2 by EPD (Ref. 20) adopting an applied potential of 10 V and a deposition time of 45 s. The obtained sample was hence annealed in air at 400°C for 1 h.

As Received Condition: as grown

Analyzed Region: same as host material

Ex Situ Preparation/Mounting: Sample was fixed by a conductive copper tape and a metallic clip on a grounded sample holder and introduced into the analysis chamber through a fast entry lock system.

In Situ Preparation: none

Charge Control: No flood gun was used during analysis.

Temp. During Analysis: 298 K

Pressure During Analysis: $<10^{-8}$ Pa

Pre-analysis Beam Exposure: 120 s.

INSTRUMENT DESCRIPTION

Manufacturer and Model: ThermoFisher Scientific Escalab Xi+

Analyzer Type: spherical sector

Detector: Channeltron

Number of Detector Elements: 6

INSTRUMENT PARAMETERS COMMON TO ALL SPECTRA

■*Spectrometer*

Analyzer Mode: constant pass energy

Throughput (T=E^N): Calculated from a polynomial fit to a plot of log[peak area/(PE×XSF)] *vs*. log[KE/PE], where PE is the pass energy, KE is the kinetic energy, and XSF is the relative sensitivity factor.

Excitation Source Window: None

Excitation Source: Al Ka monochromatic

Source Energy: 1486.6 eV

Source Strength: 225 W

Source Beam Size: 650 μm × 650 μm

Signal Mode: multichannel direct

■*Geometry*

Incident Angle: 58°

Source-to-Analyzer Angle: 58°

Emission Angle: 0°

Specimen Azimuthal Angle: 90°

Acceptance Angle from Analyzer Axis: 0°

Analyzer Angular Acceptance Width: 30° × 30°

■*Ion Gun*

Manufacturer and Model: ThermoFisher Scientific MAGCIS Ion Source

Energy: 4000 eV

Current: 7 nA

Current Measurement Method: biased stage

Sputtering Species: Ar^+

Spot Size (unrastered): 500 μm

Raster Size: 3250 μm x 3250 μm

Incident Angle: 40°

Polar Angle: 40°

Azimuthal Angle: 90°

Comment: differentially pumped ion gun

DATA ANALYSIS METHOD

Energy Scale Correction: -

Recommended Energy Scale Shift: 0 eV for all specimens

Peak Shape and Background Method: After performing a Shirley-type background subtraction (Ref. 27), BE and full width at half maximum (FWHM) values were determined by least-squares fitting adopting Gaussian/Lorentzian sum functions.

Quantitation Method: Atomic concentrations were calculated by peak area integration, using sensitivity factors provided by Thermo Scientific Avantage software.

ACKNOWLEDGMENTS

The authors acknowledge funding received from CNR (Progetti di Ricerca @CNR – avviso 2020 - ASSIST), Padova University (P-DiSC#04BIRD2020-UNIPD EUREKA, DOR 2020-2023), INSTM Consortium (INSTM21PDGASPAROTTO - NANO^{MAT}, INSTM21PDBARMAC - ATENA), AMGA Foundation (NYMPHEA project) and EPSRC (EP/V055232/1, EP/R008841/1). Thanks are also due to Dr. Andrea Gallo for his valuable experimental support.

DATA AVAILABILITY

The data that support the findings of this study are available within the article and its supplementary material.

REFERENCES

1. M. Benedet, G. A. Rizzi, A. Gasparotto, N. Gauquelin, A. Orekhov, J. Verbeeck, C. Maccato and D. Barreca, Appl. Surf. Sci. **618**, 156652 (2023).
2. L. Bigiani, D. Barreca, A. Gasparotto, T. Andreu, J. Verbeeck, C. Sada, E. Modin, O. I. Lebedev, J. R. Morante and C. Maccato, Appl. Catal., B **284**, 119684 (2021).
3. X. Chang, X. Zhai, S. Sun, D. Gu, L. Dong, Y. Yin and Y. Zhu, Nanotechnol. **28**, 135705 (2017).

4. L. Lin, H. Ou, Y. Zhang and X. Wang, ACS Catal. **6**, 3921 (2016).
5. Y. Zhao, J. Zhang, W. Wu, X. Guo, P. Xiong, H. Liu and G. Wang, Nano Energy **54**, 129 (2018).
6. M. Benedet, G. A. Rizzi, A. Gasparotto, O. I. Lebedev, L. Girardi, C. Maccato and D. Barreca, Chem. Eng J. **448**, 137645 (2022).
7. J. Huang, Y. Lu, H. Zhang, L. Shangguan, Z. Mou, J. Sun, S. Sun, J. He and W. Lei, Chem. Eng. J. **405**, 126685 (2021).
8. J. Liu, N. Y. Liu, H. Li, L. P. Wang, X. Q. Wu, H. Huang, Y. Liu, F. Bao, Y. Lifshitz, S. T. Lee and Z. H. Kang, Nanoscale **8**, 11956 (2016).
9. W. Liu, Z. Zhang, D. Zhang, R. Wang, Z. Zhang and S. Qiu, RSC Adv. **10**, 28848 (2020).
10. Z. Mo, H. Xu, Z. Chen, X. She, Y. Song, J. Lian, X. Zhu, P. Yan, Y. Lei, S. Yuan and H. Li, Appl. Catal., B **241**, 452 (2019).
11. L. Bigiani, A. Gasparotto, C. Maccato, C. Sada, J. Verbeeck, T. Andreu, J. R. Morante and D. Barreca, ChemCatChem **12**, 5984 (2020).
12. T. S. Miller, A. B. Jorge, T. M. Suter, A. Sella, F. Corà and P. F. McMillan, Phys. Chem. Chem. Phys **19**, 15613 (2017).
13. Q. Liang, Z. Li, Z.-H. Huang, F. Kang and Q.-H. Yang, Adv. Funct. Mater. **25**, 6885 (2015).
14. S. He, K. Xiao, X.-Z. Chen, T. Li, T. Ouyang, Z. Wang, M.-L. Guo and Z.-Q. Liu, J. Colloid Interf. SCi. **557**, 644 (2019).
15. X. Li, G. Fang, X. Qian and Q. Tian, Chem. Eng. J. **428**, 131052 (2022).
16. F. Dong, Z. Wang, Y. Li, W.-K. Ho and S. C. Lee, Environ. Sci. Technol. **48**, 10345 (2014).
17. L. Bigiani, T. Andreu, C. Maccato, E. Fois, A. Gasparotto, C. Sada, G. Tabacchi, D. Krishnan, J. Verbeeck, J. R. Morante and D. Barreca, J. Mater. Chem. A **8**, 16902 (2020).
18. B. P. Mishra, L. Acharya, S. Subudhi and K. Parida, Int. J. Hydrogen Energy **47**, 32107 (2022).
19. Y.-S. Jun, E. Z. Lee, X. Wang, W. H. Hong, G. D. Stucky and A. Thomas, Adv. Funct. Mater. **23**, 3661 (2013).
20. S. Zhang, J. Yan, S. Yang, Y. Xu, X. Cai, X. Li, X. Zhang, F. Peng and Y. Fang, Chin. J. Catal. **38**, 365 (2017).
21. H. Yu, R. Shi, Y. Zhao, T. Bian, Y. Zhao, C. Zhou, G. I. N. Waterhouse, L.-Z. Wu, C.-H. Tung and T. Zhang, Adv. Mater. **29**, 1605148 (2017).
22. Y. Xiao, G. Tian, W. Li, Y. Xie, B. Jiang, C. Tian, D. Zhao and H. Fu, J. Am. Chem. Soc. **141**, 2508 (2019).
23. F. Cheng, T. Zhang, Y. Zhang, J. Du, X. Han and J. Chen, Angew. Chem. Int. Ed. **52**, 2474 (2013).
24. Pattern N° 024-0735, JCPDS (2000).
25. H. Soltani, H. Bahiraei and S. Ghasemi, J. Alloys Compd. **904**, 163565 (2022).
26. C. Maccato, L. Bigiani, G. Carraro, A. Gasparotto, R. Seraglia, J. Kim, A. Devi, G. Tabacchi, E. Fois, G. Pace, V. Di Noto and D. Barreca, Chem. Eur. J. **23**, 17954 (2017).
27. D. A. Shirley, Phys. Rev. B **5**, 4709 (1972).
28. L. Bigiani, C. Maccato, D. Barreca and A. Gasparotto, Surf. Sci. Spectra **27**, 024005 (2020).
29. F. Gri, L. Bigiani, A. Gasparotto, C. Maccato and D. Barreca, Surf. Sci. Spectra **25**, 024004 (2018).
30. X. Pan, F. Kong and M. Xing, Res. Chem. Intermed. **48**, 2837 (2022).
31. J. F. Moulder, W. F. Stickle, P. E. Sobol and K. D. Bomben, *Handbook of X-ray Photoelectron Spectroscopy* (Perkin Elmer Corporation, Eden Prairie, MN, USA, 1992).
32. http://srdata.nist.gov/xps.
33. Y. Zhang, H. Li, L. Zhang, R. Gao and W.-L. Dai, ACS Sustain. Chem. Eng. **7**, 17008 (2019).
34. C. Du, Z. Zhang, S. Tan, G. Yu, H. Chen, L. Zhou, L. Yu, Y. Su, Y. Zhang, F. Deng and S. Wang, Environ. Res. **200**, 111427 (2021).
35. Z. Gu, Y. Asakura and S. Yin, Nanotechnol. **31**, 114001 (2020).
36. P. Xia, B. Zhu, B. Cheng, J. Yu and J. Xu, ACS Sustainable Chem. Eng. **6**, 965 (2018).
37. Y. Shi, M. Zhang, Y. Li, G. Liu, R. Jin, Q. Wang, H. Xu and S. Gao, Ceram. Int. **46**, 25905 (2020).
38. M. Wang, M. Shen, L. Zhang, J. Tian, X. Jin, Y. Zhou and J. Shi, Carbon **120**, 23 (2017).
39. X. Guo, J. Duan, W. Wang and Z. Zhang, Fuel **280**, 118544 (2020).
40. J. Wang and W.-D. Zhang, Electrochimica Acta **71**, 10 (2012).
41. D. J. Morgan, Surf. Sci. Spectra **28**, 014007 (2021).
42. Y. Shi, S. Gao, Y. Yuan, G. Liu, R. Jin, Q. Wang, H. Xu and J. Lu, Nano Energy **77**, 105153 (2020).
43. Q. Zhang, Y. Peng, F. Deng, M. Wang and D. Chen, Sep. Purif. Technol. **246**, 116890 (2020).
44. D. Liu, Z. Zhang and J. Wu, Energy Fuels **33**, 3089 (2019).
45. F. Mattelaer, T. Bosserez, J. Ronge, J. A. Martens, J. Dendooven and C. Detavernier, RSC Adv. **6**, 98337 (2016).
46. G. Peng, L. Xing, J. Barrio, M. Volokh and M. Shalom, Angew. Chem. Int. Ed. **57**, 1186 (2018).

SPECTRAL FEATURES TABLE

Spectrum ID #	Element/ Transition	Peak Energy (eV)	Peak Width FWHM (eV)	Peak Area (eV x cts/s)	Sensitivity Factor	Concentration (at. %)	Peak Assignment
NFigA02[a]	C 1s	284.8	1.7	10652.5	1.000	23.9	Adventitious surface contamination
NFigA02[a]	C 1s	288.0	2.1	1939.1	1.000	4.4	Adsorbed carbonates
NFigA03[b]	O 1s	529.9	1.5	35990.4	2.881	28.1	Lattice oxygen in MnO_2
NFigA03[b]	O 1s	531.5	2.0	24396.2	2.881	19.0	Surface adsorbed hydroxyl/carbonate groups
NFigA04[c]	Mn 2p	…	…	135000.7	12.353	24.6	Mn(IV) in MnO_2
NFigA04	Mn $2p_{3/2}$	642.6	2.7	…	…	…	Mn(IV) in MnO_2
NFigA04	Mn $2p_{1/2}$	654.2	2.7	…	…	…	Mn(IV) in MnO_2
NFigB02[a]	C 1s	284.8	1.7	9690.6	1.000	19.0	Adventitious surface contamination
NFigB02[a]	C 1s	286.4	2.0	1607.9	1.000	3.2	C in C-NH_x (x = 1,2) groups on gCN edges
NFigB02[a]	C 1s	288.4	2.1	3057.9	1.000	6.0	N=C-N carbon atoms in gCN aromatic rings and adsorbed carbonates
NFigB03[d]	N 1s	398.8	1.9	3852.4	1.676	4.5	Two-coordinated C=N-C nitrogen atoms in gCN
NFigB03[d]	N 1s	400.1	1.6	936.5	1.676	1.1	Tertiary N-$(C)_3$ nitrogen atoms in gCN
NFigB03[d]	N 1s	401.4	1.6	549.5	1.676	0.6	NH_x (x = 1,2) uncondensed amino groups
NFigB03[d]	N 1s	404.4	2.5	269.2	1.676	0.3	Excitation of π-electrons in gCN heptazinic rings
NFigB04[b]	O 1s	529.7	1.5	37490.9	2.881	25.5	Lattice oxygen in MnO_2
NFigB04[b]	O 1s	531.5	1.6	21724.9	2.881	14.8	Surface adsorbed hydroxyl/carbonate groups
NFigB04[b]	O 1s	532.8	1.7	2855.3	2.881	1.9	C-O-Mn bonds
NFigB05[c]	Mn 2p	…	…	145465.8	12.353	23.1	Mn(IV) in MnO_2
NFigB05	Mn $2p_{3/2}$	642.4	2.7	…	…	…	Mn(IV) in MnO_2
NFigB05	Mn $2p_{1/2}$	654.0	2.7	…	…	…	Mn(IV) in MnO_2
NFigC02[a]	C 1s	284.8	1.8	3662.2	1.000	5.8	Adventitious surface contamination
NFigC02[a]	C 1s	286.6	2.0	4657.1	1.000	7.4	C in C-NH_x (x = 1,2) groups on gCN edges
NFigC02[a]	C 1s	288.7	2.1	12849.4	1.000	20.5	N=C-N carbon atoms in gCN aromatic rings and adsorbed carbonates
NFigC03[d]	N 1s	399.1	1.8	18723.2	1.676	17.8	Two-coordinated C=N-C nitrogen atoms in gCN
NFigC03[d]	N 1s	400.3	1.6	7004.4	1.676	6.7	Tertiary N-$(C)_3$ nitrogen atoms in gCN
NFigC03[d]	N 1s	401.6	1.9	6600.3	1.676	6..3	NH_x (x = 1,2) uncondensed amino groups
NFigC03[d]	N 1s	404.6	2.4	1347.0	1.676	1.3	Excitation of π-electrons in gCN heptazinic rings
NFigC04[b]	O 1s	529.5	1.4	19516.7	2.881	10.8	Lattice oxygen in MnO_2
NFigC04[b]	O 1s	531.5	1.8	15927.9	2.881	8.8	Surface adsorbed hydroxyl/carbonate groups
NFigC04[b]	O 1s	532.8	1.8	4879.2	2.881	2.7	C-O-Mn bonds
NFigC05[c]	Mn 2p	…	…	91826.7	12.353	11.9	Mn(IV) in MnO_2
NFigC05	Mn $2p_{3/2}$	642.2	2.5	…	…	…	Mn(IV) in MnO_2
NFigC05	Mn $2p_{1/2}$	653.8	2.5	…	…	…	Mn(IV) in MnO_2

[a] The sensitivity factor is referred to the whole C 1s signal.
[b] The sensitivity factor is referred to the whole O 1s signal.
[c] The sensitivity factor, peak area, and concentration are referred to the whole Mn 2p signal.
[d] The sensitivity factor is referred to the whole N 1s signal.

Footnote to Spectra NFigA01, NFigB01 and NFigC01: Besides the occurrence of carbon-containing species arising from atmospheric exposure, the wide-scan spectrum of sample accession #MnO_2 revealed the sole signals of manganese and oxygen, indicating that the present MnO_2 deposit fully covered the Ni foam substrate. In the case of sample accessions MnO_2-gCN(M) and MnO_2-gCN(CM), MnO_2 signals were still clearly detectable but,

in addition, even the ones arising from gCN could be detected, suggesting that functionalization with carbon nitride did not produce a complete coverage of the underlying oxide.

Footnote to Spectra NFigA02, NFigB02 and NFigC02: For sample accession #MnO_2, two distinct components contributed to the C 1s signal. The main one, centered at BE = 284.8 eV, was related to adventitious carbon contamination (Refs. 28-31), while a second contribution at 288.0 eV was assigned to surface chemisorbed carbonates originating from air exposure (Refs. 28, 29, 31, 32). For sample accessions MnO_2-gCN(M) and MnO_2-gCN(CM), the C 1s peak was deconvoluted into three bands: (**i**) the former one, at BE = 284.8 eV, was related to adventitious carbon (Refs. 33, 34); (**ii**) a second component, centered at ≈ 286.5 eV, was ascribed to carbon atoms bonded to amino-groups (C-NH_x, with x = 1, 2) on the edges of gCN heptazinic rings, arising from an incomplete precursor condensation (Refs. 7, 21, 35), and also to the presence of C-O linkages between carbon nitride and manganese dioxide (Refs. 3, 8, 10, 34, 36-38), that might facilitate charge transfer among MnO_2 and gCN (Ref. 38) (see below); (**iii**) finally, a contribution at ≈ 288.5 eV was due to N-C=N carbon atoms belonging to carbon nitride aromatic rings (Refs. 3, 8-10, 16, 34, 35, 39-41). The latter band was also likely affected by the presence of adsorbed carbonates, featuring a relatively close BE value (see comment to the C1s signal for sample accession #MnO_2). Compared to previous studies on bare gCN systems and in line with results reported for analogous composite systems (Refs. 30, 34, 42), components (**ii**) and (**iii**) underwent a shift to higher BEs. Such an effect, also confirmed by the analysis of the O 1s, Mn 2p and N 1s signals (see below), appears consistent with the formation of a *Z*-scheme heterojunction, with electrons flowing from carbon nitride to MnO_2, at their interface (Ref. 15). For samples accession MnO_2-gCN(M) and MnO_2-gCN(CM), the contribution of component (**ii**) reveals an appreciable material defectivity, that might favorably affect the ultimate catalytic activity (Refs. 6, 21, 22).

Footnote to Spectra NFigA03, NFigB04 and NFigC04: Fitting of the O 1s signal for sample accession #MnO_2 revealed a main band at BE = 529.9 eV due to lattice oxygen in manganese dioxide (Refs. 10, 15, 28, 29, 31, 37, 42, 43). In the case of sample accessions MnO_2-gCN(M) and MnO_2-gCN(CM), such a component underwent a negative BE shift of -0.2 eV and -0.4 eV, respectively, if compared to the bare MnO_2 sample (Refs. 33, 36), corroborating the above discussed *Z*-scheme mechanism. The more marked shift for sample accession MnO_2-gCN(CM) *vs*. accession MnO_2-gCN(M) is likely due to the more exfoliated gCN morphology and its enhanced interfacial contact with manganese(IV) oxide, promoting charge transfer phenomena between the two semiconductors (Ref. 44). Besides the O 1s lattice component, all specimens also displayed a second band at 531.5 eV assigned to hydroxyl/carbonate species adsorbed on surface defects (Refs. 30, 33, 36). In addition, for sample accessions MnO_2-gCN(M) and MnO_2-gCN(CM), a third component at 532.8 eV was attributed to the formation of C-O-Mn bonds (Refs. 15, 36, 37, 42), and its contribution to the O 1s signal was larger for sample accession MnO_2-gCN(CM). This phenomenon, along with the more marked BE shifts of Mn and lattice oxygen peaks, highlights the formation of a more effective heterojunction for sample accession MnO_2-gCN(CM).

Footnote to Spectra NFigA04, NFigB05 and NFigC05: For sample accession #MnO_2, the Mn 2p peak features and, in particular, the Mn $2p_{3/2}$ energy position (BE = 642.6 eV) (Refs. 2, 29, 31, 42, 43) and the corresponding spin-orbit splitting (SOS) = 11.6 eV (Refs. 8, 15, 37, 42) confirmed the obtainment of MnO_2 free from other manganese oxides in appreciable amounts. This conclusion was further supported by the BE difference between Mn $2p_{3/2}$ and O 1s lattice components of 112.7 eV (Refs. 28, 29, 45). As far as composite systems are concerned, the Mn 2p signal underwent a downward shift of -0.2 eV for sample accession MnO_2-gCN(M), and -0.4 eV for sample accession MnO_2-gCN(CM) with respect to bare MnO_2. As already discussed for C 1s and O 1s signals, and in line with previous works (Refs. 14, 30, 36, 37, 42), this phenomenon confirmed once again the formation of a *Z*-scheme junction between carbon nitride and manganese dioxide and the concomitant generation of a built-in electric field at their interface (Ref. 3, 15), promoting thus the electron transfer from gCN to MnO_2, a more pronounced phenomenon for sample accession MnO_2-gCN(CM).

Footnote to Spectra NFigB03 and NFigC03: For accessions MnO_2-gCN(M) and MnO_2-gCN(CM), the N 1s signal could be fitted by means of four bands: (**i**) the main one, at BE ≈ 399.0 eV, related to gCN bi-coordinated nitrogen centers (C=N-C) (Refs. 13, 16, 38, 39, 41); (**ii**) a second component, at ≈ 400.2 eV, assigned to tri-coordinated N atoms [N-$(C)_3$] in the carbon nitride framework (Refs. 3, 9, 12, 13, 21, 35, 46); (**iii**) a further contribution, at ≈ 401.5 eV, due to the presence of uncondensed NH_x (x = 1, 2) groups (Refs. 12, 14, 21, 22, 34, 46); (**iv**) a weaker band at ≈ 404.5 eV, assigned to π-electron excitations (Refs. 3, 9, 13, 33, 43). In line with the above comments, the more effective gCN to MnO_2 electron transfer for sample accession MnO_2-gCN(CM) was further supported by the fact that the four components contributing to the N 1s peak were all shifted to higher BE values, if compared to accession MnO_2-gCN(M). For sample accession MnO_2-gCN(CM), the relative contribution of component (**iii**) to the overall N 1s signal was appreciably higher, indicating a larger content of terminal -NH_x groups and a lower degree of condensation of the used precursors during their conversion into gCN.

ANALYZER CALIBRATION TABLE							
Spectrum ID #	**Element/ Transition**	**Peak Energy (eV)**	**Peak Width FWHM (eV)**	**Peak Area (eV x cts/s)**	**Sensitivity Factor**	**Concentration (at. %)**	**Peak Assignment**
figCalib01[a]	Au $4f_{7/2}$	84.0	0.9	383688.8	…	...	Au(0)
figCalib02[a]	Cu $2p_{3/2}$	932.7	1.3	655128.5	…	...	Cu(0)

[a] The peak was acquired after Ar^+ erosion.

GUIDE TO FIGURES					
Spectrum (Accession) #	**Spectral Region**	**Voltage Shift***	**Multiplier**	**Baseline**	**Comment #**
NFigA01	Survey	0	1	0	…
NFigA02	C 1s	0	1	0	…
NFigA03	O 1s	0	1	0	…
NFigA04	Mn 2p	0	1	0	…
NFigB01	Survey	0	1	0	…
NFigB02	C 1s	0	1	0	…
NFigB03	N 1s	0	1	0	…
NFigB04	O 1s	0	1	0	…
NFigB05	Mn 2p	0	1	0	…
NFigC01	Survey	0	1	0	…
NFigC02	C 1s	0	1	0	…
NFigC03	N 1s	0	1	0	…
NFigC04	O 1s	0	1	0	…
NFigC05	Mn 2p	0	1	0	…

[*] Voltage shift of the archived (as measured) spectrum relative to the printed figure. The figure reflects the recommended energy scale correction due to a calibration correction, sample charging, flood gun, or other phenomena.

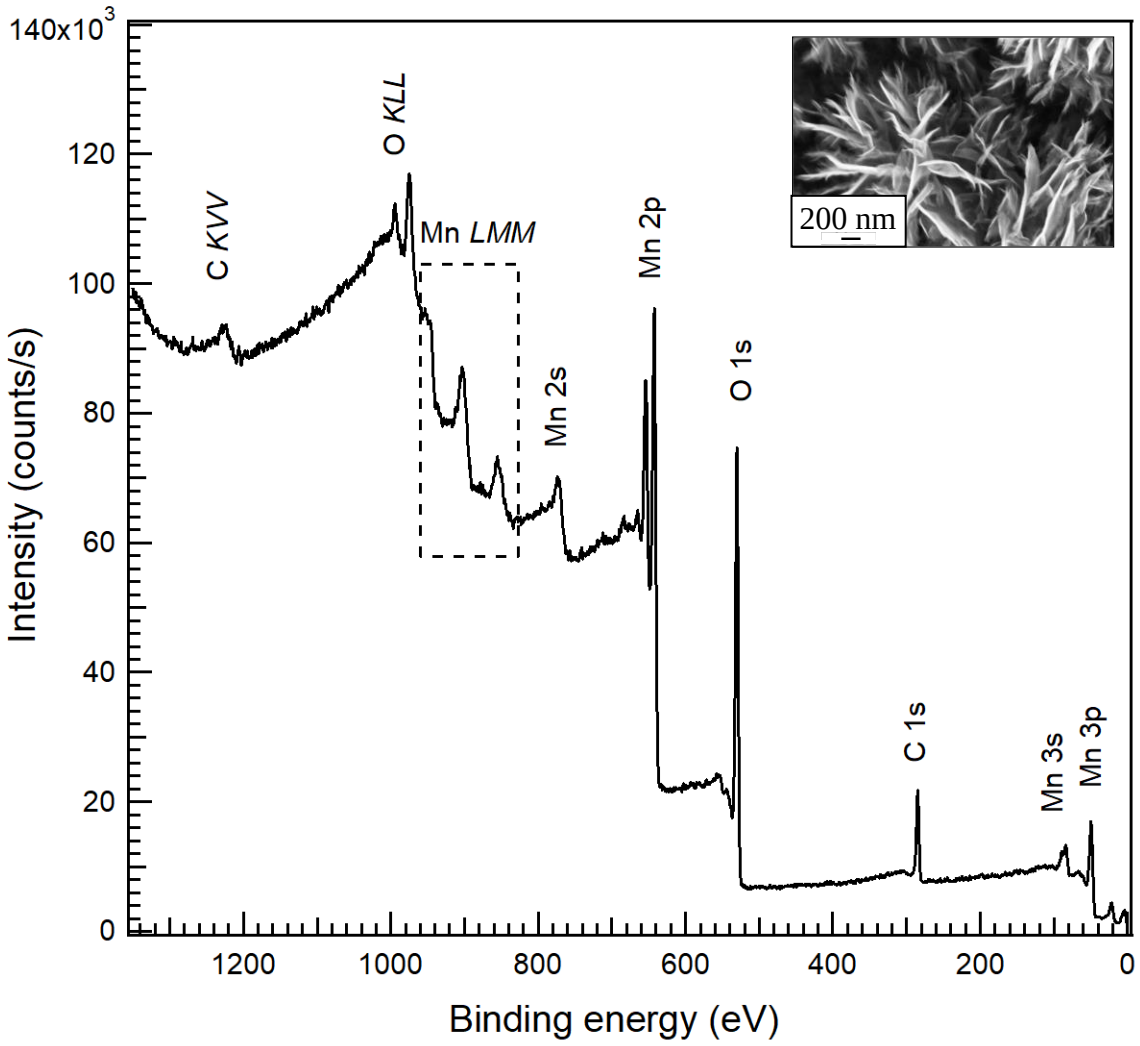

Publish in *Surface Science Spectra*: Yes ☒ No ☐

Accession #	NFigA01
Host Material	MnO_2
Technique	XPS
Spectral Region	survey
Instrument	ThermoFisher Scientific Escalab Xi+
Excitation Source	Al Ka monochromatic
Source Energy	1486.6 eV
Source Strength	225 W
Source Size	0.65 mm x 0.65 mm
Analyzer Type	spherical sector analyzer
Incident Angle	58˚
Emission Angle	0˚
Analyzer Pass Energy	187.85 eV
Analyzer Resolution	1.9 eV
Total Signal Accumulation Time	340.2 s
Total Elapsed Time	374.2 s
Number of Scans	10
Effective Detector Width	1.9 eV

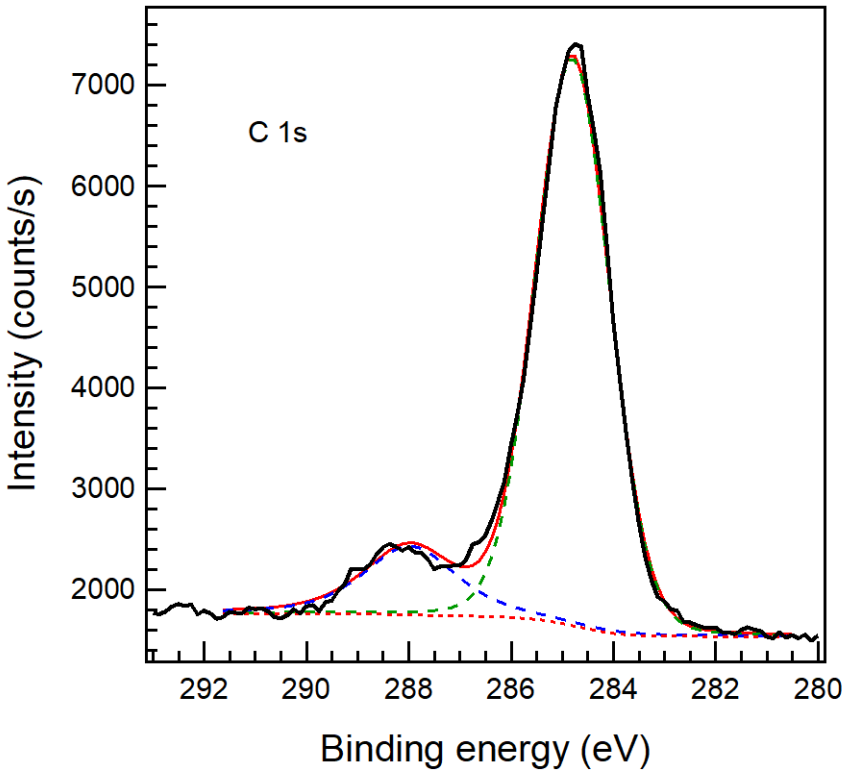

Publish in *SSS*: Yes X No ☐

- **Accession #:** NFigA02
- **Host Material:** MnO_2
- **Technique:** XPS
- **Spectral Region:** C 1s

Instrument: ThermoFisher Scientific Escalab Xi+
Excitation Source: Al Ka monochromatic
Source Energy: 1486.6 eV
Source Strength: 225 W
Source Size: 0.65 mm x 0.65 mm
Analyzer Type: spherical sector
Incident Angle: 58˚
Emission Angle: 0˚
Analyzer Pass Energy 58.7 eV
Analyzer Resolution: 0.6 eV
Total Signal Accumulation Time: 138.8 s
Total Elapsed Time: 152.6 s

Number of Scans: 15

Effective Detector Width: 0.6 eV

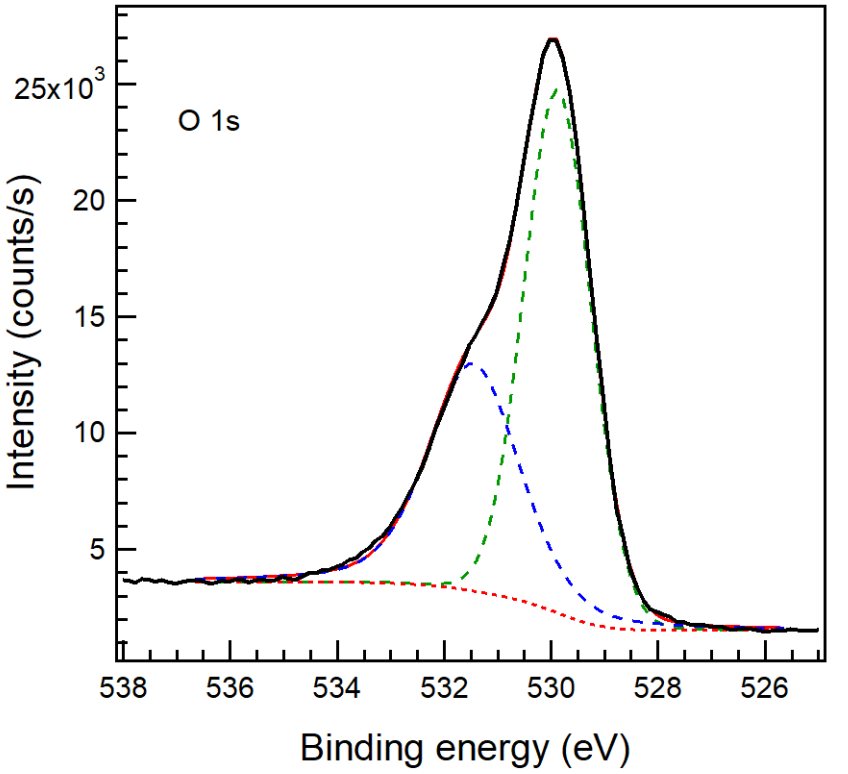

Publish in *SSS*: Yes X No ☐

- **Accession #:** NFigA03
- **Host Material:** MnO_2
- **Technique:** XPS
- **Spectral Region:** O 1s

Instrument: ThermoFisher Scientific Escalab Xi+
Excitation Source: Al Ka monochromatic
Source Energy: 1486.6 eV
Source Strength: 225 W
Source Size: 0.65 mm x 0.65 mm
Analyzer Type: spherical sector
Incident Angle: 58˚
Emission Angle: 0˚
Analyzer Pass Energy 58.7 eV
Analyzer Resolution: 0.6 eV
Total Signal Accumulation Time: 150.8 s
Total Elapsed Time: 165.8 s

Number of Scans: 15

Effective Detector Width: 0.6 eV

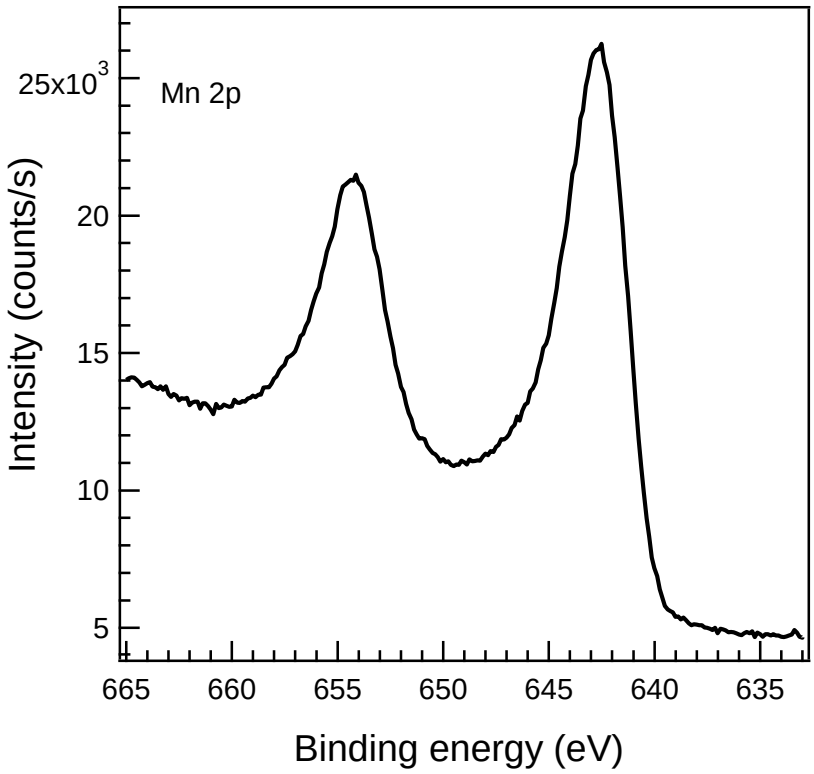

Publish in *SSS*: Yes X No ☐

- **Accession #:** NFigA04
- **Host Material:** MnO_2
- **Technique:** XPS
- **Spectral Region:** Mn 2p

Instrument: ThermoFisher Scientific Escalab Xi+
Excitation Source: Al Ka monochromatic
Source Energy: 1486.6 eV
Source Strength: 225 W
Source Size: 0.65 mm x 0.65 mm
Analyzer Type: spherical sector
Incident Angle: 58˚
Emission Angle: 0˚
Analyzer Pass Energy 58.7 eV
Analyzer Resolution: 0.6 eV
Total Signal Accumulation Time: 361.0 s
Total Elapsed Time: 397.1 s
Number of Scans: 20
Effective Detector Width: 0.6 eV

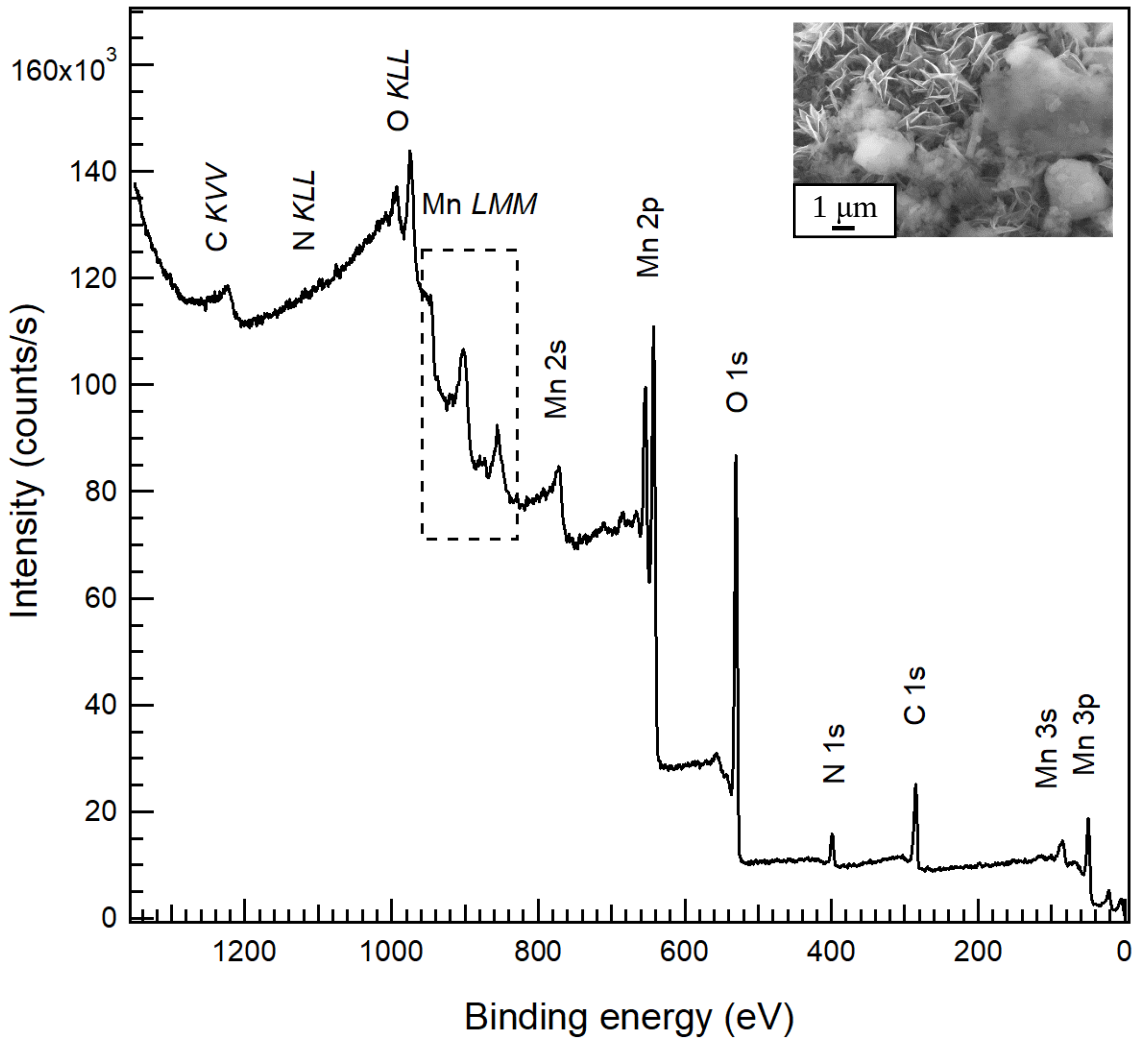

Publish in *Surface Science Spectra*: Yes ☒ No ☐

Accession #	NFigB01
Host Material	MnO_2-gCN(M)
Technique	XPS
Spectral Region	survey
Instrument	ThermoFisher Scientific Escalab Xi+
Excitation Source	Al Ka monochromatic
Source Energy	1486.6 eV
Source Strength	225 W
Source Size	0.65 mm x 0.65 mm
Analyzer Type	spherical sector analyzer
Incident Angle	58˚
Emission Angle	0˚
Analyzer Pass Energy	187.85 eV
Analyzer Resolution	1.9 eV
Total Signal Accumulation Time	340.2 s
Total Elapsed Time	374.2 s
Number of Scans	10
Effective Detector Width	1.9 eV

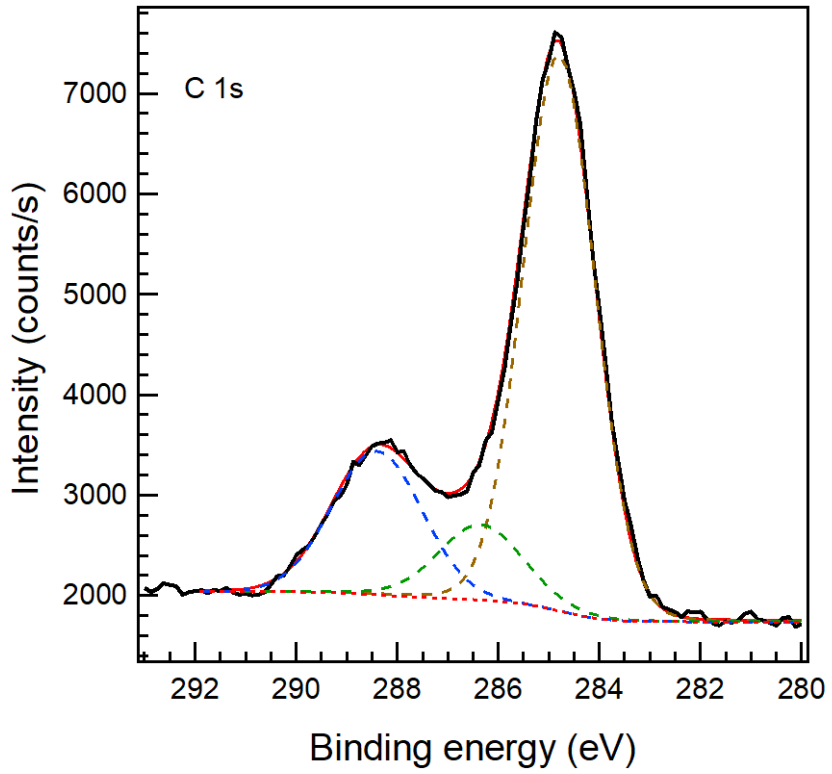

Publish in *SSS*: Yes ☒ No ☐

- **Accession #:** NFigB02
- **Host Material:** MnO_2-gCN(M)
- **Technique:** XPS
- **Spectral Region:** C 1s

Instrument: ThermoFisher Scientific Escalab Xi+
Excitation Source: Al Ka monochromatic
Source Energy: 1486.6 eV
Source Strength: 225 W
Source Size: 0.65 mm x 0.65 mm
Analyzer Type: spherical sector
Incident Angle: 58˚
Emission Angle: 0˚
Analyzer Pass Energy 58.7 eV
Analyzer Resolution: 0.6 eV
Total Signal Accumulation Time: 138.8 s
Total Elapsed Time: 152.6 s

Number of Scans: 15

Effective Detector Width: 0.6 eV

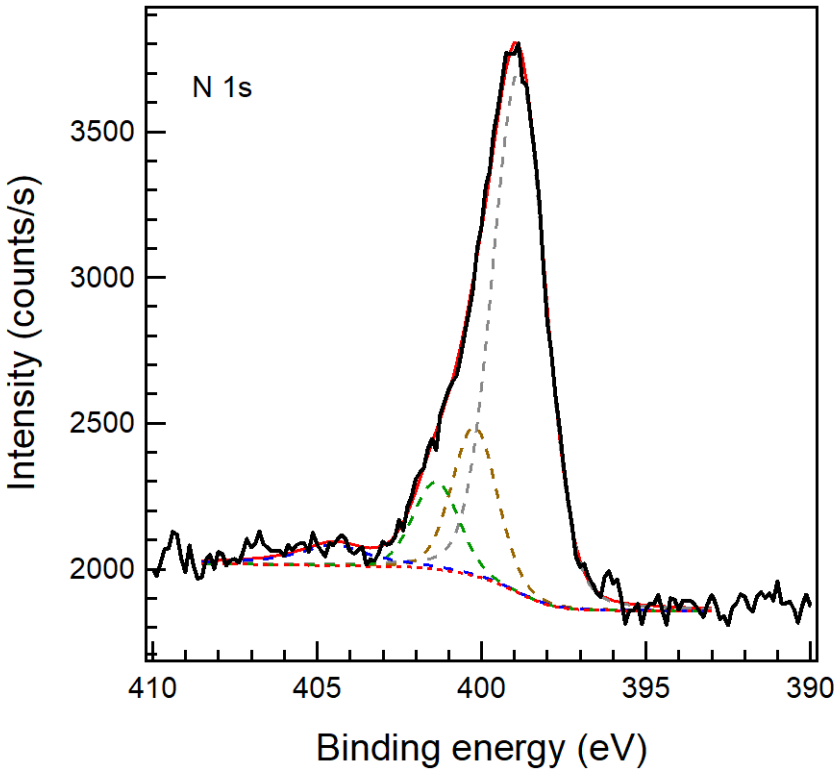

Publish in *SSS*: Yes ☒ No ☐

- **Accession #:** NFigB03
- **Host Material:** MnO_2-gCN(M)
- **Technique:** XPS
- **Spectral Region:** N 1s

Instrument: ThermoFisher Scientific Escalab Xi+
Excitation Source: Al Ka monochromatic
Source Energy: 1486.6 eV
Source Strength: 225 W
Source Size: 0.65 mm x 0.65 mm
Analyzer Type: spherical sector
Incident Angle: 58˚
Emission Angle: 0˚
Analyzer Pass Energy 58.7 eV
Analyzer Resolution: 0.6 eV
Total Signal Accumulation Time: 193.0 s
Total Elapsed Time: 212.3 s

Number of Scans: 20

Effective Detector Width: 0.6 eV

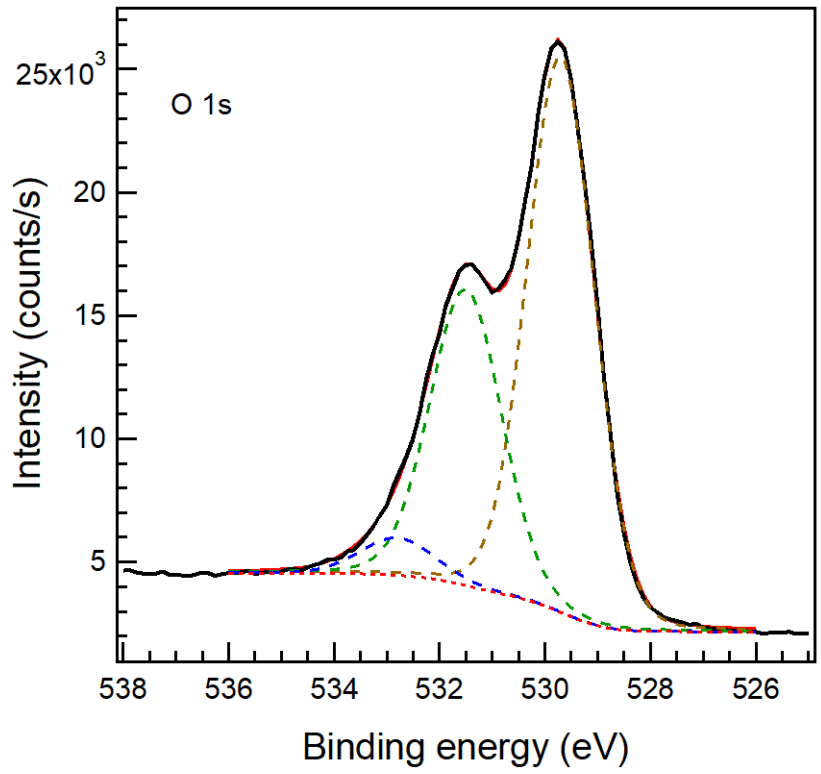

Publish in *SSS*: Yes ☒ No ☐

- **Accession #:** NFigB04
- **Host Material:** MnO_2-gCN(M)
- **Technique:** XPS
- **Spectral Region:** O 1s

Instrument: ThermoFisher Scientific Escalab Xi+
Excitation Source: Al Ka monochromatic
Source Energy: 1486.6 eV
Source Strength: 225 W
Source Size: 0.65 mm x 0.65 mm
Analyzer Type: spherical sector
Incident Angle: 58˚
Emission Angle: 0˚
Analyzer Pass Energy 58.7 eV
Analyzer Resolution: 0.6 eV
Total Signal Accumulation Time: 150.8 s
Total Elapsed Time: 165.8 s

Number of Scans: 15

Effective Detector Width: 0.6 eV

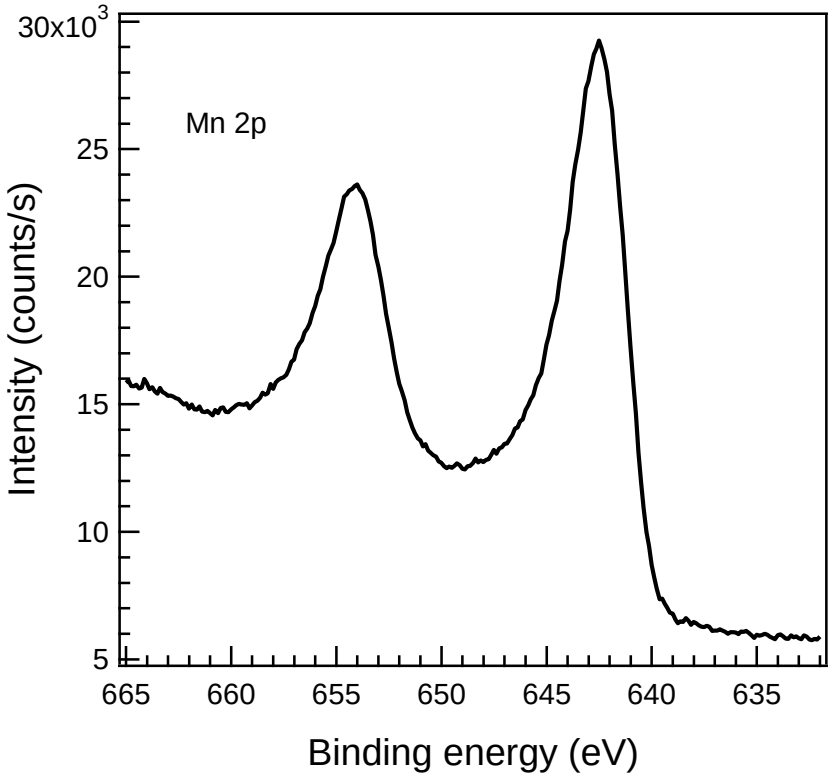

Publish in *SSS*: Yes ☒ No ☐

- **Accession #:** NFigB05
- **Host Material:** MnO_2-gCN(M)
- **Technique:** XPS
- **Spectral Region:** Mn 2p

Instrument: ThermoFisher Scientific Escalab Xi+
Excitation Source: Al Ka monochromatic
Source Energy: 1486.6 eV
Source Strength: 225 W
Source Size: 0.65 mm x 0.65 mm
Analyzer Type: spherical sector
Incident Angle: 58˚
Emission Angle: 0˚
Analyzer Pass Energy 58.7 eV
Analyzer Resolution: 0.6 eV
Total Signal Accumulation Time: 361.0 s
Total Elapsed Time: 397.1 s

Number of Scans: 20

Effective Detector Width: 0.6 eV

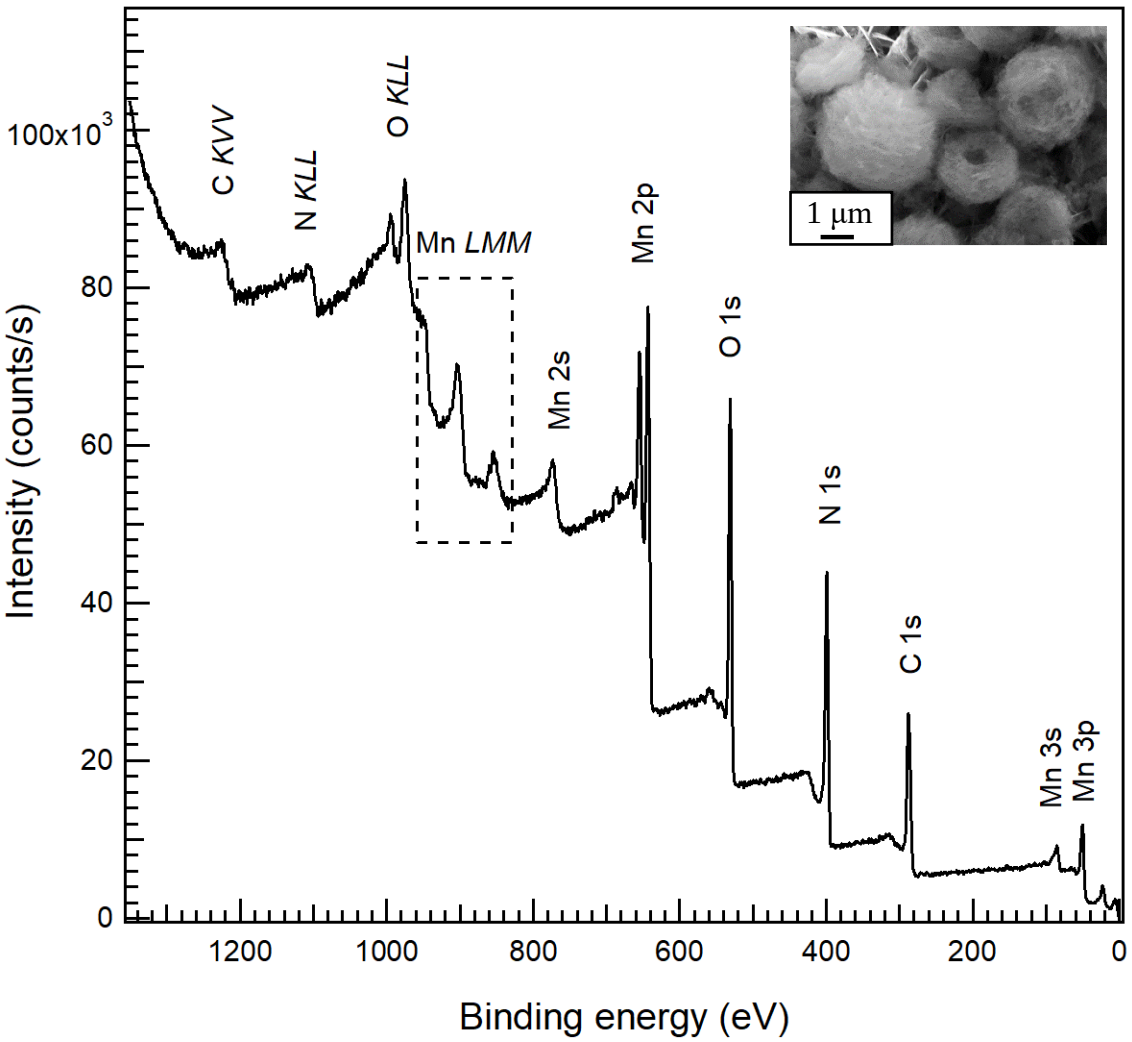

Publish in *Surface Science Spectra*: Yes ☒ No ☐

Accession #	NFigC01
Host Material	MnO_2-gCN(CM)
Technique	XPS
Spectral Region	survey
Instrument	ThermoFisher Scientific Escalab Xi+
Excitation Source	Al Ka monochromatic
Source Energy	1486.6 eV
Source Strength	225 W
Source Size	0.65 mm x 0.65 mm
Analyzer Type	spherical sector analyzer
Incident Angle	58˚
Emission Angle	0˚
Analyzer Pass Energy	187.85 eV
Analyzer Resolution	1.9 eV
Total Signal Accumulation Time	340.2 s
Total Elapsed Time	374.2 s
Number of Scans	10
Effective Detector Width	1.9 eV

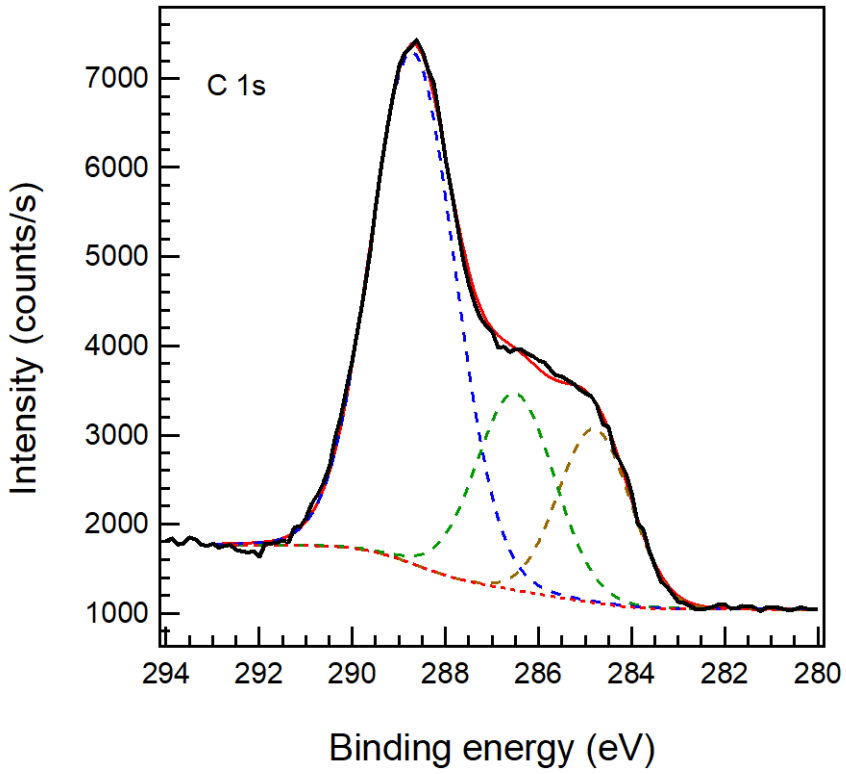

Publish in *SSS*: Yes ☒ No ☐

- **Accession #:** NFigC02
- **Host Material:** MnO_2-gCN(CM)
- **Technique:** XPS
- **Spectral Region:** C 1s

Instrument: ThermoFisher Scientific Escalab Xi+
Excitation Source: Al Ka monochromatic
Source Energy: 1486.6 eV
Source Strength: 225 W
Source Size: 0.65 mm x 0.65 mm
Analyzer Type: spherical sector
Incident Angle: 58˚
Emission Angle: 0˚
Analyzer Pass Energy 58.7 eV
Analyzer Resolution: 0.6 eV
Total Signal Accumulation Time: 138.8 s
Total Elapsed Time: 152.6 s

Number of Scans: 15

Effective Detector Width: 0.6 eV

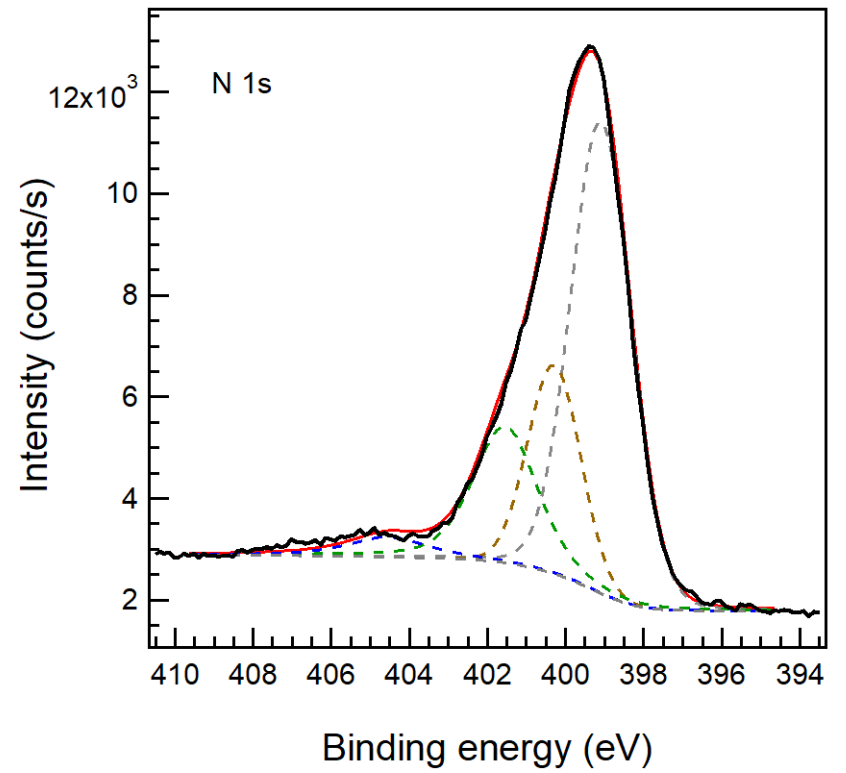

Publish in *SSS*: Yes ☒ No ☐

- **Accession #:** NFigC03
- **Host Material:** MnO_2-gCN(CM)
- **Technique:** XPS
- **Spectral Region:** N 1s

Instrument: ThermoFisher Scientific Escalab Xi+
Excitation Source: Al Ka monochromatic
Source Energy: 1486.6 eV
Source Strength: 225 W
Source Size: 0.65 mm x 0.65 mm
Analyzer Type: spherical sector
Incident Angle: 58˚
Emission Angle: 0˚
Analyzer Pass Energy 58.7 eV
Analyzer Resolution: 0.6 eV
Total Signal Accumulation Time: 193.0 s
Total Elapsed Time: 212.3 s

Number of Scans: 20

Effective Detector Width: 0.6 eV

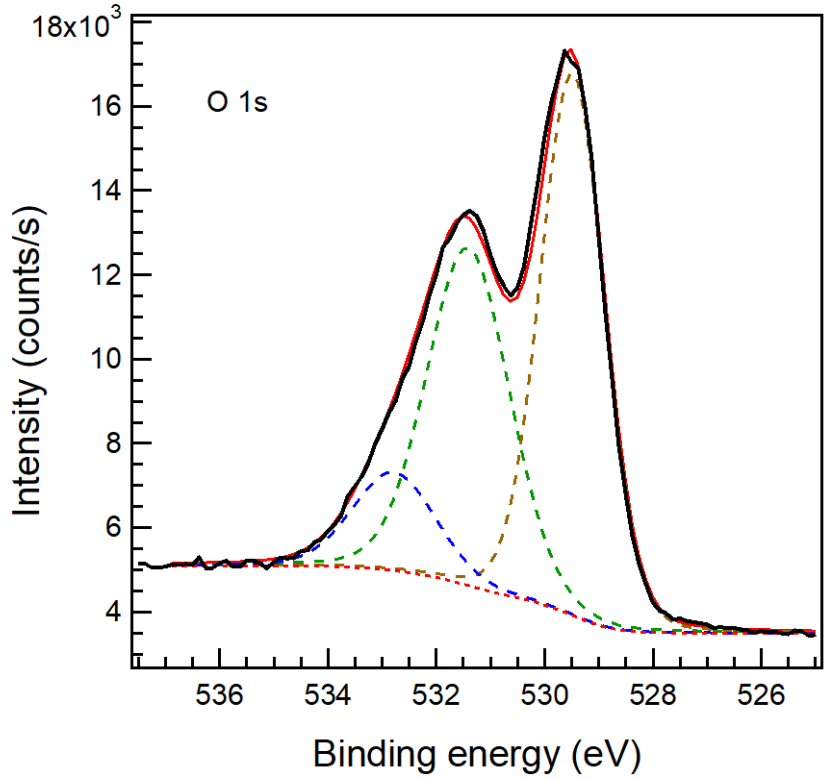

Publish in *SSS*: Yes ☒ No ☐

- **Accession #:** NFigC04
- **Host Material:** MnO_2-gCN(CM)
- **Technique:** XPS
- **Spectral Region:** O 1s

Instrument: ThermoFisher Scientific Escalab Xi+
Excitation Source: Al Ka monochromatic
Source Energy: 1486.6 eV
Source Strength: 225 W
Source Size: 0.65 mm x 0.65 mm
Analyzer Type: spherical sector
Incident Angle: 58˚
Emission Angle: 0˚
Analyzer Pass Energy 58.7 eV
Analyzer Resolution: 0.6 eV
Total Signal Accumulation Time: 150.8 s
Total Elapsed Time: 165.8 s

Number of Scans: 15

Effective Detector Width: 0.6 eV

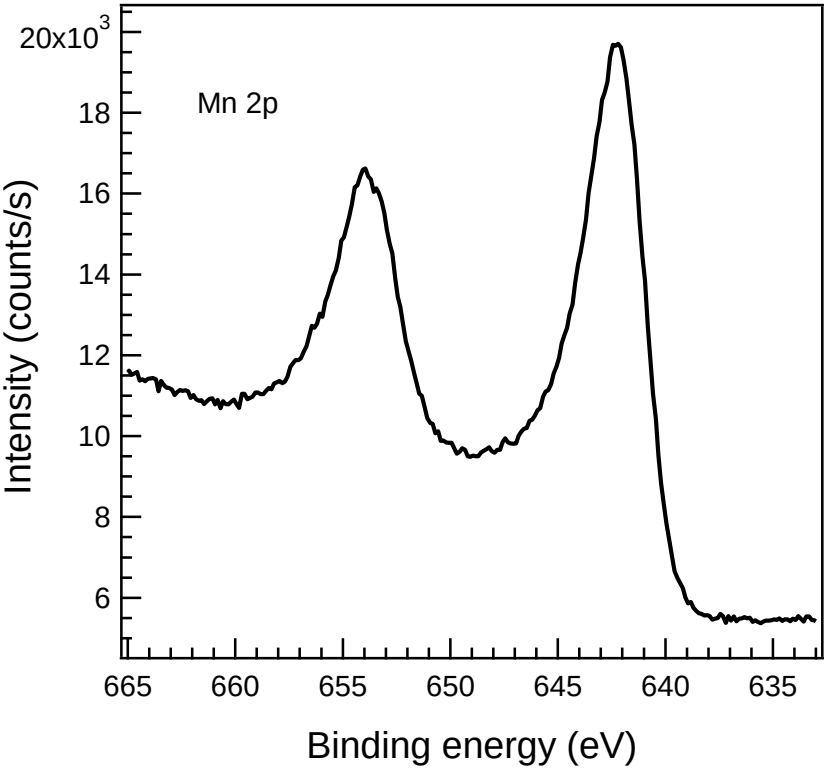

Publish in *SSS*: Yes ☒ No ☐

- **Accession #:** NFigC05
- **Host Material:** MnO_2-gCN(CM)
- **Technique:** XPS
- **Spectral Region:** Mn 2p

Instrument: ThermoFisher Scientific Escalab Xi+
Excitation Source: Al Ka monochromatic
Source Energy: 1486.6 eV
Source Strength: 225 W
Source Size: 0.65 mm x 0.65 mm
Analyzer Type: spherical sector
Incident Angle: 58˚
Emission Angle: 0˚
Analyzer Pass Energy 58.7 eV
Analyzer Resolution: 0.6 eV
Total Signal Accumulation Time: 361.0 s
Total Elapsed Time: 397.1 s

Number of Scans: 20

Effective Detector Width: 0.6 eV